JOURNAL OF GUIDANCE, CONTROL, AND DYNAMICS
Vol. 21, No. 5, September–October 1998

# Pilot-Induced Oscillations Involving Multiple Nonlinearities

Mark R. Anderson*
*Virginia Polytechnic Institute and State University, Blacksburg, Virginia 24061-0203*

**A pilot-induced oscillation is a type of instability caused by dynamic coupling between the pilot and the aircraft. Linear system analysis reveals that the pilot/aircraft system is unstable during the oscillation event. However, nonlinearities in the feedback system can limit the response variables so that a sustained, constant amplitude limit cycle results. A method is presented to analyze the limit cycle behavior of pilot/aircraft systems as a means of understanding pilot-induced oscillations and their causes. A new computational technique is considered and a new method of testing limit cycle stability is presented. An analysis of the YF-12 pilot-induced oscillation characteristics is used to demonstrate the method.**

## Introduction

A PILOT-INDUCED oscillation (PIO) is a complicated interaction between a pilot and aircraft that leads to a sustained, and sometimes very large-amplitude, oscillation of the aircraft. It is inherently characterized by a loss of stability margin in the pilot/aircraft feedback system. The oscillation can occur with motions about any or all of the aircraft's axes of symmetry. The oscillations can also lead to destruction of the aircraft.

Many flight test accidents have been attributed to PIO problems.[1] Most recently, both the YF-22 and JAS-39 Gripen prototypes have crashed as a result of PIO incidents.[2,3] Commercial aircraft also are not immune to PIO problems.[4] These recent incidents, however, appear to be the result of multiple nonlinearities acting simultaneously that lead to a loss of stability margin. Examples of these dynamic phenomena include control system mode switching, control surface rate limiting, nonlinear pilot control stick gradients, and stability augmentation system (SAS) limiting. Many of these dynamic phenomena have been treated separately. For example, several approaches to dealing with control surface rate limiting have been recently published.[5–7]

Traditional methods for analyzing PIO tendencies do not consider the effect of several nonlinear dynamic effects acting simultaneously.[8] In addition, modern aircraft tend to have more inherent motion coupling so that the pilot is required to control multiple degrees of freedom at the same time. Therefore, new methods are needed to study PIO behavior for multiaxis flying tasks with many nonlinear dynamic effects.

For many years, a PIO has been considered a special case of nonlinear limit cycling.[9] A limit cycle is a sustained oscillation of a nonlinear system. The dynamics associated with pilot/aircraft interaction are fundamentally nonlinear. In fact, both the pilot and aircraft are very complicated nonlinear systems. Thus, limit cycle analysis for systems with multiple nonlinearities is fundamental to the development of new PIO analysis and prediction methods.

Anderson and Page[10] have recently completed a study of multivariable describing function methods applied to the PIO problem. Their work considers the effect of several, isolated nonlinear elements on the limit cycle behavior of the pilot and aircraft closed-loop system. Once a model of the pilot is developed, the closed-loop system equations are formed, and numerical algorithms are used to search for limit cycle solutions. The nonlinear elements studied included actuator surface limiting and stability augmentation system limiting. They were very successful in confirming PIO susceptibility in the F-4 (degraded control system), M2-F2, and other NT-33 test configurations with known PIO characteristics.[10,11]

Received June 2, 1997; presented as Paper 97-3501 at the AIAA Atmospheric Flight Mechanics Conference, New Orleans, LA, Aug. 11–13, 1997; revision received March 23, 1998; accepted for publication April 20, 1998. 

*Associate Professor, Department of Aerospace and Ocean Engineering. Senior Member AIAA.

There are numerous advantages to the analysis method developed by Anderson and Page. First, several nonlinearities can be investigated simultaneously. This phenomenon appears to be the cause of many of the recent PIO incidents. Furthermore, the nonlinearities can appear anywhere in the pilot/aircraft closed-loop system. The nonlinearities might be associated with the pilot, the aircraft, the flight control system, or the hydraulic actuators. Last, the analysis method reveals not only an estimate of the oscillation frequency, but also the amplitudes of each signal in the feedback loop. Therefore, large-amplitude oscillations that could lead to dangerous flying characteristics are readily identified.

This paper represents a continuation of work by Anderson and Page. In particular, a new limit cycle search algorithm is presented in this paper that provides an alternative to the homotopy algorithm studied in Ref. 11. The new algorithm involves a searching technique that can be readily adapted to a common optimization framework and, therefore, does not require specialized numerical techniques. Also, a new limit cycle stability result is derived in this paper. The stability condition is very easy to calculate and provides important information about the limit cycle behavior. Finally, results of a new case study of the YF-12 aircraft are presented.

## Pilot and Control Stick Modeling

During a sustained PIO, the pilot's behavior and response are intricately coupled with the dynamics of the airplane. Therefore, to study PIO tendencies, consideration of human pilot dynamics is essential. There are several possible analytical approaches to pilot modeling that can be considered, including the classical crossover models and the more recent optimal control models. For this application, a simple gain and lag filter will be used to represent the human pilot. This model is similar to model proposed by Smith.[12] The lag filter in this case can represent either the pilot's neuromuscular dynamics or the pilot's inherent time delay. The lag filter will represent that the pilot cannot provide significant control input at higher frequencies. The time constant of the pilot lag can vary among different pilots. Typically, the lag time constant is chosen from 0 to 0.2 s.

The dynamics of the control stick or manipulator also play a very important role in analyzing the PIO tendency of an airplane. The control stick provides the interface between the pilot and the aircraft and, therefore, it provides the interface between the coupling of the two dynamic systems.

For many modern aircraft, the control stick consists of dynamic elements shown in Fig. 1. Here it is assumed that the pilot reacts to an attitude response error and applies a force input to the control manipulator. The control stick has a force breakout of typically less than 5 lb. The feel system converts the force command into a control stick deflection. Its dynamics are usually represented by a second-order filter. The natural frequency of the feel system is typically less than 30 rad/s.

The control stick obviously has maximum and minimum deflection limits. The final control stick position is sent to the flight control system. For older aircraft, the control stick position moved the

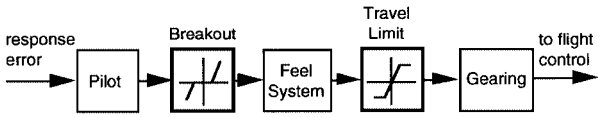


**Fig. 1 Typical control stick model.**

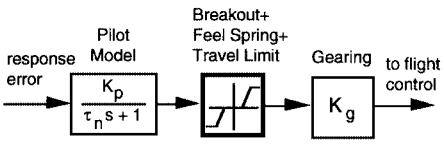


**Fig. 2 Control stick and pilot model.**

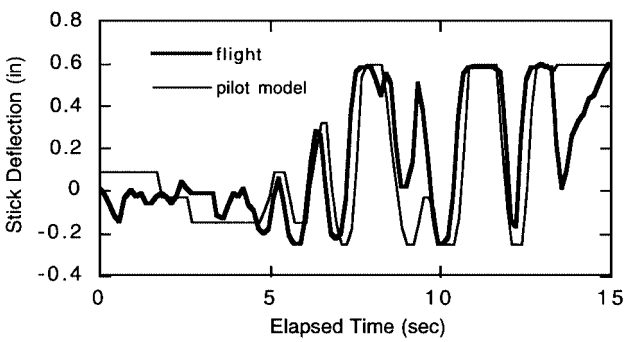


**Fig. 3 Control stick deflection from the YF-22 PIO.**

control surfaces directly and so a gearing mechanism was utilized. Modern fly-by-wire aircraft typically use a stick position sensor to create an analog or digital signal that is passed to the flight control computers electronically.

The control stick model shown in Fig. 1 includes two nonlinear elements, the breakout and the stick travel limits. Because the dynamic feel system lies between these two nonlinear elements, it is possible to study these nonlinearities individually. However, to reduce the complexity of the model, the dynamics of the feel system will be neglected. The two nonlinear elements will be combined into one element. The combined element is shown graphically in the simplified control stick and pilot model shown in Fig. 2. This model will be used in subsequent analysis.

During a sustained PIO event, the pilot will increase the gain to a level that is significantly higher than normal. If the event occurs near the ground or near other airplanes, one would expect the pilot to apply abrupt control inputs in an attempt to quickly regain a steady flight condition.

It is a difficult task to determine the appropriate pilot gain factor to represent the pilot in such an agitated state. However, a rough estimate of the pilot gain can be obtained using data from previous PIO events involving significant nonlinear effects. The thick line in Fig. 3 shows the pilot's longitudinal control stick deflection history of the YF-22 aircraft measured during the PIO event described in Ref. 2. The thin line in Fig. 2 shows the stick deflection predicted by the pilot model in Fig. 2 with $K_p = 6$ lb/deg. To generate the predicted stick deflection, it is assumed that the pilot is reacting to the measured pitch attitude of the airplane in an open-loop sense. The pilot gain was simply chosen so that the predicted stick deflection approximately matched the measured stick deflection. A force gradient of $K_s = 60$ lb/in. was used, and stick travel limits of $+0.6$ and $-0.25$ in. were assumed.

Figure 3 reveals that the predicted control stick deflection matches the actual stick deflection with a reasonable degree of accuracy. The pilot gain of 6 lb/deg is probably much larger than the pilot normally uses to control the aircraft. However, one can see from Fig. 3 that the pilot gain might be changing with time as well. Nevertheless, in later analysis, we will consider pilot gains greater than this value as possibly occurring during a sustained PIO event.

## Limit Cycle Determination

Describing functions offer a useful way to analyze the effect of multiple nonlinearities in a feedback diagram. To search for limit cycle behavior using the describing function approach, the nonlinear elements of the pilot/vehicle system must be isolated. The system can then be separated into two parts. One part is completely linear and the other part includes only memoryless nonlinearities such as the deadbands and limiters described earlier.

Assume that the linear portion of the system includes an input vector $\boldsymbol{u}$ and an output vector $\boldsymbol{y}$. The following state-space model will be used to represent this dynamic model:

$$\dot{\boldsymbol{x}} = F\boldsymbol{x} + G\boldsymbol{u} \tag{1}$$

$$\boldsymbol{y} = H\boldsymbol{x} \tag{2}$$

Note that the preceding state-space model can contain parts of the aircraft, pilot, actuators, or control system. In other words, the linear model state variables can come from several or all of these subsystems.

The nonlinear elements in the feedback system will be replaced by their single-input, sinusoidal, describing functions. The function from $\boldsymbol{y}$ to $\boldsymbol{u}$ represents the quasilinear part of the system and is represented by

$$\boldsymbol{u} = N(\boldsymbol{y})\boldsymbol{y} \tag{3}$$

where $N(\boldsymbol{y})$ is a diagonal matrix of describing functions. Each quasilinear describing function depends on the amplitude of the signal entering the nonlinear element. For example, the (1,1) element of $N(\boldsymbol{y})$ depends on the amplitude of the signal $y_1(t)$ and so on.

Combining the linear and quasilinear equations leads to the set of homogeneous closed-loop system equations

$$\dot{\boldsymbol{x}} = A\boldsymbol{x} \tag{4}$$

where $A = F + GN(\boldsymbol{y})H$. These closed-loop equations are used to search for limit cycle behavior.

We are interested in oscillatory solutions of the form $x(t) = \mathrm{Re}\{\boldsymbol{X}e^{j\omega t}\}$, where $\boldsymbol{X}$ is a vector of complex phasors and $\omega$ is the limit cycle or PIO frequency. By taking the time derivative of $x(t)$ and substituting into the closed-loop system equations, the following equation results:

$$\mathrm{Re}\{j\omega\boldsymbol{X}e^{j\omega t}\} = A\,\mathrm{Re}\{\boldsymbol{X}e^{j\omega t}\} \tag{5}$$

When the describing function matrix $N(\boldsymbol{y})$ stems from static, odd-symmetric nonlinear elements, $N(\boldsymbol{y})$ will be real and, therefore, $A$ will be real. The closed-loop equations can then be written as

$$\mathrm{Re}\{j\omega\boldsymbol{X}e^{j\omega t}\} = \mathrm{Re}\{A\boldsymbol{X}e^{j\omega t}\} \tag{6}$$

One can see from this expression that an oscillatory solution is found if $\boldsymbol{X}$ and $\omega$ satisfy

$$j\omega\boldsymbol{X} = A\boldsymbol{X} \tag{7}$$

This sufficient condition for the existence of limit cycle behavior is very similar to an eigenvector/eigenvalue decomposition of the matrix $A$. A solution is found when the matrix $A$ has imaginary roots of $\pm j\omega$. However, recall that $A$ depends on $N(\boldsymbol{Y})$ and $\boldsymbol{Y}$ depends on $\boldsymbol{X}(\boldsymbol{Y} = H\boldsymbol{X})$, and so the equation is very nonlinear and sometimes difficult to solve.

There are several algorithms available to search for limit cycles. Some use the earlier described condition and attempt to determine the conditions where the eigenvalues of $A$ are purely imaginary.[13–16] Other techniques search for only the real and imaginary parts of the vector $\boldsymbol{Y}$ directly.[17–21] Almost all of the existing algorithms are iterative methods because both solution approaches lead to a set of nonlinear equations.

If a good initial guess of the solution can be obtained, a gradient-based function minimization algorithm can be used to yield an exact solution. Because the phasor vector $\boldsymbol{X}$ is complex, let

$$\boldsymbol{X} = \boldsymbol{X}_R + j\boldsymbol{X}_I \tag{8}$$

The sufficient condition for existence of a limit cycle becomes

$$j\omega(\boldsymbol{X}_R + j\boldsymbol{X}_I) = A(\boldsymbol{X}_R + j\boldsymbol{X}_I) \tag{9}$$

or, combining real and imaginary terms,

$$(A\boldsymbol{X}_R + \omega\boldsymbol{X}_I) + j(A\boldsymbol{X}_I - \omega\boldsymbol{X}_R) = 0 \tag{10}$$

An objective function can be chosen as the magnitude of the given complex vector equation. A limit cycle solution is found if $V = 0$ with

$$V = \boldsymbol{a}^T\boldsymbol{a} + \boldsymbol{b}^T\boldsymbol{b} \tag{11}$$

where $\boldsymbol{a} = A\boldsymbol{X}_R + \omega\boldsymbol{X}_I$ and $\boldsymbol{b} = A\boldsymbol{X}_I - \omega\boldsymbol{X}_R$ are both real vectors.

Many gradient-based function minimization algorithms can be used to find the minimum value of $V$ as it is defined in Eq. (11). The unknown parameters of the problem are the elements of $\boldsymbol{X}_R$ and $\boldsymbol{X}_I$ along with the limit cycle frequency $\omega$. However, because the phase angles in $\boldsymbol{X}$ can be expressed relative to one another, one can arbitrarily set one element of either $\boldsymbol{X}_R$ or $\boldsymbol{X}_I$ to zero. The problem then has $2n$ unknowns including the frequency $\omega$ (where $n$ is the dimension of $x$).

A reasonable initial solution can be found using the eigenvector/eigenvalue decomposition of $A$ and guesses for $N(\boldsymbol{Y})$. When $N(\boldsymbol{Y})$ models only saturation nonlinearities, the magnitude of the describing functions in $N(\boldsymbol{Y})$ will vary between zero and unity. $N(\boldsymbol{Y})$ equal to the identity matrix indicates that no limiting is occurring. One can then change the diagonal elements of $N(\boldsymbol{Y})$ from unity to zero to represent increased levels of limiting.

Once $N(\boldsymbol{Y})$ is chosen, the matrix $A$ can be found along with its eigenvalues and eigenvectors. Recall that a limit cycle is found if $A$ has a pair of eigenvalues that are purely imaginary. Therefore, reasonable initial solutions are found by simply varying $N(\boldsymbol{Y})$ and checking the eigenvalues of $A$. If a complex eigenvalue pair is found with relatively small real parts, an initial guess for $\boldsymbol{X}$ is the eigenvector associated with this imaginary eigenvalue pair. Note that the eigenvector may need to be scaled so that $\boldsymbol{Y} = H\boldsymbol{X}$ yields magnitudes in $\boldsymbol{Y}$ that are consistent with the initial guess for $N(\boldsymbol{Y})$. The initial guess of the limit cycle frequency would be the imaginary part of the nearly imaginary eigenvalue.

## Limit Cycle Stability

The state trajectory $x(t)$ of a stable limit cycle will return to the limit cycle after it has been perturbed away from it. The state trajectory of an unstable limit cycle will not return to its solution after perturbation. Most PIOs are sustained for several cycles, so that stable limit cycles in the pilot/vehicle system are sought. Because the limit cycle is predicted when one pair of eigenvalues is purely imaginary, we are interested in finding how the real part of the eigenvalues change when the solution is perturbed.

Consider the spectral decomposition of $A$ given by

$$A = \sum_{k=1}^{n} \lambda_k \boldsymbol{u}_k \boldsymbol{v}_k^T \tag{12}$$

where the right eigenvectors $\boldsymbol{u}_k$ satisfy $\lambda_k\boldsymbol{u}_k = A\boldsymbol{u}_k$ and the left eigenvectors $\boldsymbol{v}_k^T$ satisfy $\boldsymbol{v}_k^T\lambda_k = \boldsymbol{v}_k^T A$. By definition of the earlier spectral decomposition, the left and right eigenvectors are normalized so that $\boldsymbol{v}_k^T\boldsymbol{u}_k = 1$.

Assume that the $i$th complex eigenvalue defines the limit cycle solution, i.e., $\lambda_i = \sigma + j\omega$ (but $\sigma$ is equal to zero at the limit cycle solution). The $i$th right eigenvector $\boldsymbol{u}_i$ is proportional to the limit cycle phasor $\boldsymbol{X}$. Premultiply the equation $\lambda_i\boldsymbol{u}_i = A\boldsymbol{u}_i$ by $\boldsymbol{v}_i^T$ to yield

$$\lambda_i \boldsymbol{v}_i^T\boldsymbol{u}_i = \boldsymbol{v}_i^T A\boldsymbol{u}_i \tag{13}$$

Now suppose that $A$ depends on a small perturbation parameter $\rho$. Take partial derivatives of Eq. (13) with respect to $\rho$:

$$\frac{\partial\lambda_i}{\partial\rho}\boldsymbol{v}_i^T\boldsymbol{u}_i + \lambda_i\frac{\partial\boldsymbol{v}_i^T}{\partial\rho}\boldsymbol{u}_i + \lambda_i\boldsymbol{v}_i^T\frac{\partial\boldsymbol{u}_i}{\partial\rho} = \frac{\partial\boldsymbol{v}_i^T}{\partial\rho}A\boldsymbol{u}_i + \boldsymbol{v}_i^T\frac{\partial A}{\partial\rho}\boldsymbol{u}_i + \boldsymbol{v}_i^T A\frac{\partial\boldsymbol{u}_i}{\partial\rho} \tag{14}$$

Combining terms, we see that

$$\frac{\partial\lambda_i}{\partial\rho}\boldsymbol{v}_i^T\boldsymbol{u}_i = \boldsymbol{v}_i^T\frac{\partial A}{\partial\rho}\boldsymbol{u}_i + \frac{\partial\boldsymbol{v}_i^T}{\partial\rho}(A\boldsymbol{u}_i - \lambda_i\boldsymbol{u}_i) + \left(\boldsymbol{v}_i^T A - \lambda_i\boldsymbol{v}_i^T\right)\frac{\partial\boldsymbol{u}_i}{\partial\rho} \tag{15}$$

By the definitions of $\boldsymbol{u}_i$ and $\boldsymbol{v}_i$, we note that the last two terms of expression (15) are equal to zero. The new expression becomes

$$\frac{\partial\lambda_i}{\partial\rho}\boldsymbol{v}_i^T\boldsymbol{u}_i = \boldsymbol{v}_i^T\frac{\partial A}{\partial\rho}\boldsymbol{u}_i \tag{16}$$

and, because the eigenvectors are normalized so that $\boldsymbol{v}_i^T\boldsymbol{u}_i = 1$, we get

$$\frac{\partial\lambda_i}{\partial\rho} = \boldsymbol{v}_i^T\frac{\partial A}{\partial\rho}\boldsymbol{u}_i \tag{17}$$

Finally, because we will only be interested in the real part of the eigenvalue $\sigma$, its partial derivative becomes

$$\frac{\partial\sigma}{\partial\rho} = \mathrm{Re}\left\{\boldsymbol{v}_i^T\frac{\partial A}{\partial\rho}\boldsymbol{u}_i\right\} \tag{18}$$

To use this result to test for limit cycle stability, assume that the amplitude of the output phasor $\boldsymbol{Y}$ is perturbed by an amount $\partial\rho$. This positive perturbation essentially moves the state trajectory outside of the limit cycle solution. When the solution is perturbed outside the existing limit cycle, the eigenvalue associated with a stable limit cycle should have a negative real part so that the trajectory will shrink and return to the limit cycle.

Once $\boldsymbol{Y}$ is perturbed, the matrix $A$ will also be perturbed through $N(\boldsymbol{Y})$. By the definition of $A$, it should be clear that the partial derivative of $A$ with respect to $\rho$ is given by

$$\frac{\partial A}{\partial\rho} = G\frac{\partial N(\boldsymbol{Y})}{\partial\rho}H \tag{19}$$

Replacing this partial in Eq. (18) yields the final stability condition

$$\frac{\partial\sigma}{\partial\rho} = \mathrm{Re}\left\{\boldsymbol{v}_i^T G\frac{\partial N(\boldsymbol{Y})}{\partial\rho}H\boldsymbol{u}_i\right\} \tag{20}$$

A stable limit cycle requires $\partial\sigma/\partial\rho < 0$. A positive perturbation $\partial\rho > 0$ moves the trajectory outside the existing limit cycle and requires a negative change in the real part of the eigenvalue $\partial\sigma < 0$ to move the trajectory back to the limit cycle. Conversely, an unstable limit cycle will have $\partial\sigma/\partial\rho > 0$. This stability requirement is the same as those reported by other researchers.[13,14,16] However, the condition provided earlier is very easy to check due to the particular construction of the state-space model. The eigenvectors of $A$ are readily available when checking the limit cycle solution. The partial of $N(\boldsymbol{Y})$ with respect to $\rho$ can be computed analytically or numerically using a finite difference scheme.

## Example

The YF-12 was a forerunner of the SR-71 reconnaissance airplane. In the early 1970s, NASA pilots experienced PIO tendencies during aerial refueling of this airplane.[22] There were two distinct tendencies noticed by the YF-12 pilots. One type of PIO was described by the pilots as a bobbling motion at the cockpit that was presumably caused by the flexing of the aircraft. The oscillations were of small magnitude, but tended to be bothersome. The oscillations also tended to worsen as fuel was taken onboard the aircraft. This oscillation tendency was characterized by pilot longitudinal control stick inputs of less than 3 deg peak-to-peak. The control inputs were continuous, particularly during the final portion of the refueling task. The oscillation frequency was estimated to be approximately 6 rad/s. This frequency is hard to confirm from the recorded aircraft responses because the oscillations were very small.

A large amplitude PIO was also experienced on at least two occasions. One event was triggered by an overshoot of the longitudinal trim system. The pilot took abrupt action to correct the trim overrun just before hookup. The ensuing pitch oscillation lasted for several cycles. Unfortunately, the aircraft had very limited instrumentation so that only a few variables were recorded. The oscillation frequency for this large-amplitude PIO is about 4 rad/s.

Figure 4 shows a PIO analysis diagram that is appropriate for the longitudinal axis of the YF-12 airplane. Note that two nonlinear elements are modeled. The first nonlinear element $N_1(y_1)$ represents the breakout and the control stick travel limit. The control stick breakout is $b_1 = 5$ lb, the travel limit is $d_1 = 25$ lb, and the feel spring constant is $K_s = 0.5$ deg/lb. The gearing gain is $K_g = 0.74$ deg/deg. As already discussed, a nonlinear element combining the breakout and stick travel limits will be used for this analysis. The describing function for this element is[23]

$$N_1(Y_1) = K_s[f(\gamma_2) - f(\gamma_1)] \tag{21}$$

where $\gamma_1 = b_1/R_1$, $\gamma_2 = d_1/R_1$ and $R_1$ is the amplitude of $y_1$, i.e., $R_1 = |Y_1|$. The saturation function $f(\gamma)$ is given by

$$f(\gamma) = (2/\pi)[\sin^{-1}\gamma + \gamma\sqrt{1-\gamma^2}] \qquad |\gamma| \le 1 \tag{22}$$

For stability analysis, one also needs the partial of the describing function with respect to the signal amplitude. In this case, the (1,1) element of $\partial N(\boldsymbol{Y})/\partial\rho$ is

$$\frac{\partial N_1(Y_1)}{\partial\rho} = \frac{4K_s}{\pi R_1}\left[\gamma_1\sqrt{1-\gamma_1^2} - \gamma_2\sqrt{1-\gamma_2^2}\right] \tag{23}$$

The second nonlinear element $N_2(\boldsymbol{y}_2)$ models the limiter placed on the output of the lead/lag stability augmentation filter. The SAS limits the feedback commands to $d_2 = 2.5$ deg. The describing function for this element is

$$N_2(Y_1) = f(\gamma_3) \tag{24}$$

where $\gamma_3 = d_2/R_2$ and $R_2 = |Y_2|$. The partial derivative of this describing function is

$$\frac{\partial N_2(Y_2)}{\partial\rho} = -\frac{4\gamma_3}{\pi R_2}\sqrt{1-\gamma_3^2} \tag{25}$$

The flight condition of interest is Mach 0.77 at an altitude of 25,000 ft. The transfer functions modeling the airplane, actuator, and lead/lag SAS filter are, respectively,

$$G_p(s) = \frac{6(s+0.8)}{s(s^2+1.5s+4)} + \frac{5.17}{s^2+1.57s+246}\left[\frac{\text{deg}}{\text{deg}}\right] \tag{26}$$

$$G_h(s) = \frac{6(s+0.8)}{s^2+1.5s+4}\left[\frac{\text{deg}}{\text{deg/s}}\right] \tag{27}$$

$$A(s) = \frac{34}{s+34}\left[\frac{\text{deg}}{\text{deg}}\right] \tag{28}$$

$$H(s) = \frac{0.375(s+8)}{(s+4)}\left[\frac{\text{deg}}{\text{deg}}\right] \tag{29}$$

A state-space model that represents the linear part of the YF-12 block diagram is shown in Table 1. The state vector for this model is

$$x = \begin{bmatrix} \text{angle-of-attack (deg)} \\ \text{pitch rate (deg/s)} \\ \text{pitch attitude (deg)} \\ \text{flex pitch attitude (deg)} \\ \text{flex pitch rate (deg/s)} \\ \text{elevon (deg)} \\ \text{pilot lag (deg)} \\ \text{SAS lag (deg)} \end{bmatrix} \tag{30}$$

The SAS lag state variable is associated with the SAS filter $H(s)$ and the elevon state variable stems from the elevon actuator $A(s)$. The pilot lag state variable comes from the lag pilot model shown in Fig. 4. The input vector $\boldsymbol{u}^T = [u_1 \;\; u_2]$ and output vector $\boldsymbol{y}^T = [y_1 \;\; y_2]$ are labeled and defined in Fig. 4 as well.

Figure 5 shows the limit cycle frequencies that are found when the pilot gain and lag time constants are varied. There are essentially two types of limit cycles predicted. The solutions labeled low frequency have oscillation frequencies on the order of 4–6 rad/s, whereas those labeled high frequency oscillate at nearly 16 rad/s.

The solid curves in Fig. 5 represent stable limit cycles, whereas the dashed curves are unstable limit cycles. As an example, Fig. 5 reveals that both a stable and an unstable limit cycle exist for a pilot gain of 20 lb/deg and a lag time constant of 0.15 s. For comparison, Table 2 lists the stability properties associated with these two limit cycles. The value of the describing functions $N_1(y_1)$ and $N_2(y_2)$

**Table 1 State-space model for YF-12 PIO analysis**

$$F = \begin{bmatrix} -0.904 & 1.0 & 0 & 0 & 0 & 0.18 & 0 & 0 \\ -3.486 & -0.609 & 0 & 0 & 0 & 6.084 & 0 & 0 \\ 0 & 1.0 & 0 & 0 & 0 & 0 & 0 & 0 \\ 0 & 0 & 0 & 0 & 1.0 & 0 & 0 & 0 \\ 0 & 0 & 0 & -246.49 & -1.57 & 5.176 & 0 & 0 \\ 0 & 0 & 0 & 0 & 0 & -34.0 & 0 & 0 \\ 0 & 0 & 1/\tau_n & 1/\tau_n & 0 & 0 & -1/\tau_n & 0 \\ 0 & 0.375 & 0 & 0 & 0 & 0 & 0 & -4.0 \end{bmatrix}$$

$$G = \begin{bmatrix} 0 & 0 \\ 0 & 0 \\ 0 & 0 \\ 0 & 0 \\ 0 & 0 \\ 25.16 & -34.0 \\ 0 & 0 \\ 0 & 0 \end{bmatrix}$$

$$H = \begin{bmatrix} 0 & 0 & 0 & 0 & 0 & 0 & -K_p & 0 \\ 0 & 0.375 & 0 & 0 & 0 & 0 & 0 & 4.0 \end{bmatrix}$$

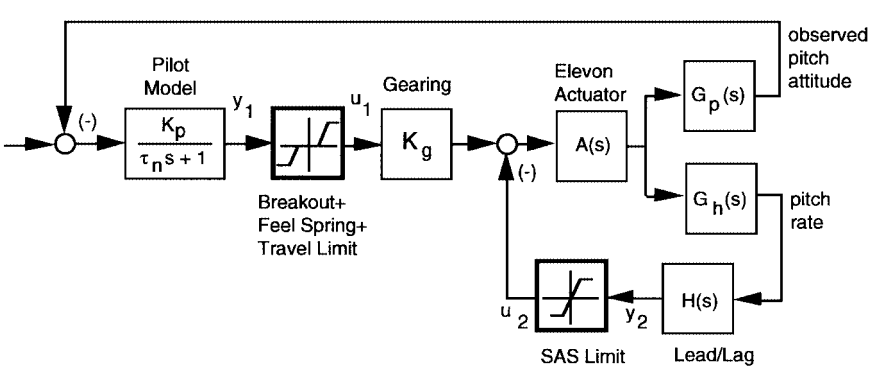


**Fig. 4 YF-12 PIO analysis diagram.**

**Table 2 Limit cycle stability properties ($K_p$ = 20 lb/deg and $\tau_n$ = 0.15 s)**

| Parameter | Stable limit cycle | Unstable limit cycle |
|---|---|---|
| $N_1(y_1)$ | 0.17 | 0.34 |
| $N_2(y_2)$ | 0.30 | 0.77 |
| Closed-loop | −0.65 | −0.72 |
| eigenvalues | −3.78 | −3.67 |
| | $0.00 \pm j3.90$ | $0.00 \pm j5.04$ |
| | −8.88 | −10.56 |
| | $-0.63 \pm j15.67$ | $-0.46 \pm j15.68$ |
| | −33.17 | −31.88 |
| $\partial\sigma/\partial\rho$ | +0.03 | +0.23 |

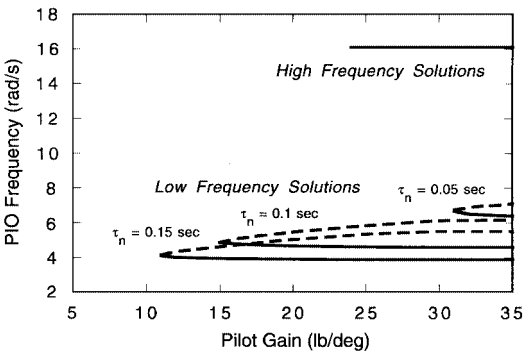


**Fig. 5 Predicted limit cycle frequencies.**

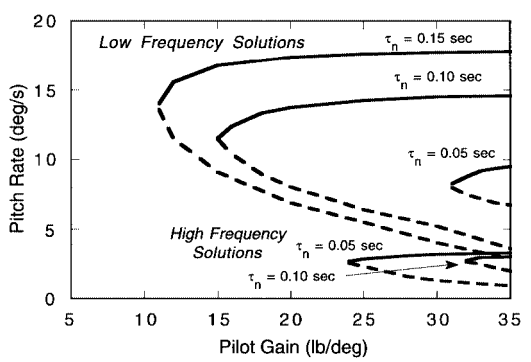


**Fig. 6 Predicted aircraft pitch rate amplitude.**

are listed first in Table 2. These values reveal that stable limit cycle yields a much higher level of signal saturation than the unstable case. This result indicates that the signal amplitudes of the stable limit cycle will be larger than the unstable limit cycle.

Next, Table 2 lists the eight system eigenvalues for each limit cycle. From the eigenvalue list, one can confirm that the stable limit cycle will oscillate at frequency near 3.9 rad/s because of the purely imaginary eigenvalue pair located at this frequency. Similarly, the unstable limit cycle will oscillate at about 5.0 rad/s. Note that all of the rest of the eigenvalues are stable (negative real part) in each case.

The stability parameter $\partial\sigma/\partial\rho$ also is listed in Table 2 for the two limit cycle solutions. As expected, the stability parameter of the unstable limit cycle has a large positive value (+0.23). However, the stability parameter of the stable-limit-cycle case is also slightly positive (+0.03). Based on the stability parameter alone, one might then assume that both limit cycles are unstable. Nonlinear simulations (presented later) confirm that indeed the stable limit cycle is stable. The error in predicting limit cycle stability is because the describing function analysis is only an approximation of the actual nonlinear system behavior. Therefore, the stability predictions based on the stability parameter $\partial\sigma/\partial\rho$ are not exact and can sometimes be conservative.

Figure 6 shows the aircraft pitch rate amplitude for each limit cycle. From this graph, one can see that low-frequency pitch rate oscillation amplitudes of greater than 15 deg/s are possible for pilot gains as low as 10 lb/deg. In general, the amplitudes of the stable oscillations increase as pilot gain increases. Also, it should be obvious that the amplitudes of the high-frequency solutions are much smaller than the low-frequency limit cycles.

Figure 6 also reveals the mechanism through which the YF-12 pilots apparently experienced both low- and high-frequency PIOs. When the lag time constant is small, a larger pilot gain is needed to cause a low-frequency limit cycle. This characteristic means that the pilot can perform much tighter tracking without worry of exciting the low-frequency limit cycles. However, the opposite is true for the high-frequency solutions. A lower pilot gain is needed to excite a high-frequency limit cycle when the pilot's lag time constant is small. Consequently, for a large but fixed pilot gain, either a low- or high-frequency solution is possible depending on the lag time constant. For example, consider the case where the pilot's gain is 30 lb/deg. A lag time constant of 0.05 s yields a high-frequency, low-amplitude limit cycle. A lag of 0.10 s leads to a low-frequency, high-amplitude limit cycle.

Figure 7 shows the low-frequency, large-amplitude oscillation that is obtained when $K_p = 20$ lb/deg and $\tau_n = 0.15$ s. The thin line shows the limit cycle obtained by a nonlinear simulation of the pilot/aircraft system shown in Fig. 4. A 6-deg pitch attitude offset has been added to the simulated pilot/aircraft system to match the trim offset of the aircraft response recorded in flight (thick line). Note that the amplitudes of both pitch attitude and pitch rate are consistent with the flight record. The largest difference in these time responses is the rate at which the oscillations grow in amplitude from the initial conditions. It appears that the flight data reaches the limit cycle conditions much quicker than the simulated data. The growth rate, however, is largely dependent on the pilot gain and may be difficult to match using a constant gain pilot model.

The oscillation frequency is 3.9 rad/s for this low-frequency case. Figure 8 shows the vertical acceleration that was recorded in flight (thick line) compared to the simulated time response (thin line). One can see from Fig. 8 that the limit cycle frequency compares well with PIO frequency of 4.2 rad/s that was experienced in flight.

The pitch rate amplitude experienced by the aircraft during the high-frequency PIO events were less than about 3 deg/s. Figure 9 shows the high-frequency limit cycle that is possible when $K_p =$ 30 lb/deg and $\tau_n = 0.05$ s. This limit cycle was very difficult to simulate because, after a nonzero initial pitch attitude, the system tends to be attracted to the nearby low-frequency limit cycle. However, if a 15 rad/s oscillating disturbance is added to the aircraft response and is held for 5 s and released, the pilot/aircraft system eventually

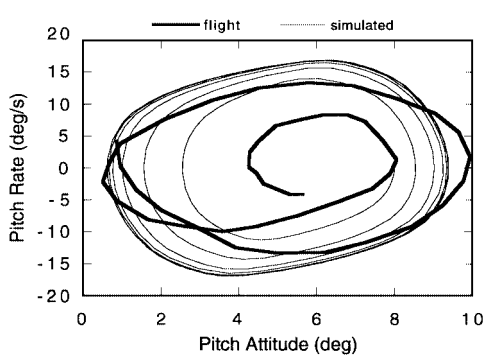


**Fig. 7 Predicted limit cycle ($K_p$ = 20 lb/deg and $\tau_n$ = 0.15 s) and measured pitch attitude/rate characteristics.**

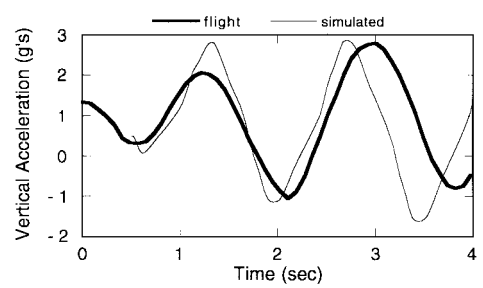


**Fig. 8 Predicted limit cycle ($K_p$ = 20 lb/deg and $\tau_n$ = 0.15 s) and measured vertical acceleration.**

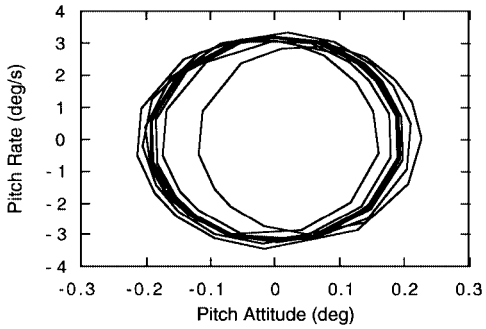


**Fig. 9 Predicted high-frequency limit cycle ($K_p$ = 30 lb/deg and $\tau_n$ = 0.05 s).**

settles into the limit cycle shown in Fig. 9. Note that the amplitudes of the high-frequency limit cycle are very small but are consistent with the values reported in flight. The oscillation frequency of this case is nearly 16 rad/s.

## Conclusion

Analyzing limit cycle characteristics for systems with multiple nonlinearities is a valuable technique for the study of PIOs. The nonlinearities inherent in the pilot's control stick dynamics can act in conjunction with other system nonlinearities such as actuator or stability-augmentation system limits to set up conditions for limit cycles to exist. The technique presented not only confirms the amplitude of the oscillations but also the frequency of the oscillations. A new computational method is also presented to estimate limit cycle stability.

Analysis of the YF-12 aircraft revealed that both high- and low-frequency PIOs are possible. The low-frequency oscillations are associated with large-amplitude motion and relatively low pilot gains. The high-frequency oscillations are characterized by very small aircraft responses, high pilot gains, and small pilot lag time constants. The results also confirmed that some combinations of pilot gain and lag lead to two possible stable limit cycles. Which limit cycle would occur in practice would depend on the initial conditions that were experienced. The characteristics of these limit cycles closely matched the reported flight test experiences.

## Acknowledgment

This effort is sponsored by the Aircraft Division, Naval Air Warfare Center, under Contract N60921-89-D-A239 (053).

## References

[1]Anderson, S. B., "Lessons Learned from a Historical Look at Flight Testing," NASA Tech Briefs, ARC-13330, Feb. 1995.

[2]Dornheim, M. A., "Report Pinpoints Factors Leading to YF-22 Crash," *Aviation Week and Space Technology*, Vol. 137, No. 19, 1992, pp. 53, 54.

[3]Butterworth-Hayes, P., "Gripen Crash Raises Canard Fears," *Aerospace America*, Vol. 32, No. 2, 1994, pp. 10, 11.

[4]Dornheim, M. A., and Hughes, D., "Boeing Corrects Several 777 PIO's," *Aviation Week and Space Technology*, Vol. 142, No. 19, 1995, p. 32.

[5]Klyde, D. H., McRuer, D. T., and Myers, T. T., "Pilot-Induced Oscillation Analysis and Prediction with Actuator Rate Limiting," *Journal of Guidance, Control, and Dynamics*, Vol. 20, No. 1, 1997, pp. 81–89.

[6]Duda, H., "Prediction of Pilot-in-the-Loop Oscillations Due to Rate Saturation," *Journal of Guidance, Control, and Dynamics*, Vol. 20, No. 3, 1997, pp. 581–587.

[7]Hess, R. A., "Unified Theory for Aircraft Handling Qualities and Adverse Aircraft-Pilot Coupling," *Journal of Guidance, Control, and Dynamics*, Vol. 20, No. 6, 1997, pp. 1141–1148.

[8]McKay, K., "Summary of an AGARD Workshop on Pilot Induced Oscillation," *AIAA Guidance, Navigation, and Control Conference* (Scottsdale, AZ), AIAA, Washington, DC, 1994, pp. 1151–1161; also AIAA Paper 94-3668, Aug. 1994.

[9]Graham, D., and McRuer, D., "Retrospective Essay on Nonlinearities in Aircraft Flight Control," *Journal of Guidance, Control, and Dynamics*, Vol. 14, No. 6, 1991, pp. 1089–1099.

[10]Anderson, M. R., and Page, A., "Multivariable Analysis of Pilot-in-the-Loop Oscillations," *AIAA Guidance, Navigation, and Control Conference* (Baltimore, MD), AIAA, Washington, DC, 1995, pp. 278–287; also AIAA Paper 95-3203, Aug. 1995.

[11]Page, A. B., and Anderson, M. R., "A Multivariable PIO Analysis of the M2-F2 Lifting Body," AIAA Paper 96-3747, July 1996.

[12]Smith, R. H., "Predicting and Validating Fully-Developed PIO," *AIAA Guidance, Navigation, and Control Conference* (Scottsdale, AZ), AIAA, Washington, DC, 1994, pp. 1162–1166; also AIAA Paper 94-3669, Aug. 1994.

[13]Aberibigbe, A. A., and Hedrick, J. K., "Limit Cycle Computation and Stability for Multivariable Nonlinear Systems," *American Control Conference* (San Diego, CA), Inst. of Electrical and Electronics Engineers, Piscataway, NJ, 1984, pp. 803–807.

[14]Abel, S. G., and Cooperrider, N. K., "An Equivalent Linearization Algorithm for Nonlinear System Limit Cycle Analysis," *Journal of Dynamic Systems, Measurement, and Control*, Vol. 107, June 1985, pp. 117–122.

[15]Pillai, V. K., and Nelson, H. D., "On an Extension of the Describing Function Method," *American Control Conference* (Atlanta, GA), Inst. of Electrical and Electronics Engineers, Piscataway, NJ, 1988, pp. 2168–2173.

[16]Pillai, V. K., and Nelson, H. D., "A New Algorithm for Limit Cycle Analysis of Nonlinear Control Systems," *Journal of Dynamic Systems, Measurement, and Control*, Vol. 110, No. 3, 1988, pp. 272–277.

[17]Mees, A., "Describing Functions, Circle Criteria and Multiple-Loop Feedback Systems," *IEE Proceedings*, Vol. 120, No. 1, 1973, pp. 126–130.

[18]Taylor, J. H., "Applications of a General Limit Cycle Analysis Method for Multivariable Systems," *Nonlinear System Analysis and Synthesis, Vol. 2: Techniques and Applications*, American Society of Mechanical Engineers, New York, 1979, pp. 143–159.

[19]Gray, J. O., and Nakhla, N. B., "Prediction of Limit Cycles in Multivariable Nonlinear Systems," *IEE Proceedings*, Vol. 128, Pt. D, No. 5, 1981, pp. 233–241.

[20]McNamara, O. P., and Atherton, D. P., "An Iterative Method for Limit Cycle Determination," *Control '85* (Cambridge, England, UK), Inst. of Electrical Engineers, London, 1985, pp. 252–257 (IEE Paper 252).

[21]Chang, H. C., Pan, C. T., Huang, C. L., and Wei, C. C., "A General Approach for Constructing the Limit Cycle Loci of Multiple-Nonlinearity Systems," *IEEE Transactions on Automatic Control*, Vol. AC-32, No. 9, 1987, pp. 845–848.

[22]Smith, J. W., and Berry, D. T., "Analysis of Longitudinal Pilot-Induced Oscillation Tendencies of the YF-12 Aircraft," NASA TND-7900, Feb. 1975.

[23]Gelb, A., and Vander Velde, W. E., *Multiple Input Describing Functions and Nonlinear System Design*, McGraw–Hill, New York, 1968, p. 523.